Electrically induced orientational instability of the director in a homeotropic nematic liquid crystal cell and its effect on surface plasmon oscillations

Ivan Yakovkin, Mykhailo Ledney

Taras Shevchenko National University of Kyiv, Faculty of Physics

ABSTRACT
This study examines the electric field-induced orientational instability of the director in a homeotropically oriented nematic liquid crystal (NLC) cell. Transitions from homogeneous homeotropic state to non-homogeneous state, and from non-homogeneous to homogeneous planar state were investigated. These transitions have a threshold and may exhibit hysteresis. Threshold voltages for these transitions were calculated and regions of existence of hysteresis were determined depending on the cell parameters. Increasing anchoring energy narrows hysteresis range for homeotropic to non-homogeneous transition and expands it for planar to non-homogeneous transition. The impact of the external electric field on the conditions and parameters of surface plasmon polariton (SPP) propagation in the Au–polymer film–NLC system was theoretically investigated. The effective refractive index of the SPP was found to increase with increasing anchoring energy of the NLC with the polymer film and with decreasing wavelength and applied voltage.

KEYWORDS
Orientational instability, nematic liquid crystal, hysteresis, surface plasmon polariton, effective refractive index.

1. Introduction

Recent advancements in nematic liquid crystal (NLC) physics have led to widespread utilization of NLCs in various fields owing to their unique electro-optical and magneto-optical properties, particularly as a fundamental element in electro-optical and display devices. Such properties of NLCs are closely related to the orientational ordering of mesophase, which significantly depends on the conditions for the director on the boundary of the cell. The influence of the substrate due to the interaction of NLC molecules with it spreads into the bulk of NLC, resulting in a certain orientational arrangement of the entire sample. The high sensitivity of NLC to external electric, magnetic and light fields opens up wide opportunities for significant control of the orientational ordering of mesophase, and as a result, the structural properties of the entire sample.

The main phenomenon behind the practical use of NLCs is the threshold orientational instability of the director. This instability can occur due to an external electric/magnetic field (known as the Fréedericksz transition) [1] or due to light (the optical

---

Fréedericksz transition [2–5]). Both transitions are types of phase transitions that may exhibit bistability [6–10] and multistability [11,12] effects. Ongoing studies include the potential use of NLC layers as control elements in photonic crystals [13,14], waveguides [15], as well as the possibility of controlling the Fréedericksz transition using electrically controlled surface coupling [16–18].

Addition of a thin layer of metal, in particular, gold, and an optical prism with a high refractive index to the thin polymer film, which is one of the bounding substrates of a plane NLC cell, allows for generation of surface plasmon-polaritons (SPPs) at the metal-polymer interface. SPP excitation at the metal-NLC interface was first demonstrated in [19]. High sensitivity of the NLC to the influence of external fields opens wide opportunities for manipulation of the SPP propagation properties. In particular, [20] demonstrated the possibility of controlling the SPP wave vector by reorienting the NLC with an applied voltage. The authors of [21,22] used SPP as a detector of the director angle near the NLC surface, establishing that an accurate description of the NLC requires rejection of the approximation of absolutely rigid anchoring. The ability to control the SPP dispersion using NLC systems opens up a variety of ways of practical application of the latter such as a spatial light modulator [23], a spectral filter [24–26] and a grating with tunable transmittance [27]. A thin layer of polyvinylcarbazole (PVK) has recently become widely used as a polymer film, which opens up the additional possibility of controlling the SPP characteristics by changing the illumination due to photorefraction. This expands the possibilities of using photorefractive NLC cells in various types of spatial light modulators [28], beam couplers [29,30]. A number of works [31–34] were devoted to the study of the influence of the electric field induced reorientation of the director in hybrid and planar NLC cells on the characteristics (in particular, the value of the refractive index) of SPP propagation. Particularly, [31] developed a theoretical approach for studying the peculiarities of SPP propagation in a three-layer system consisting of metal, PVK, and hybrid oriented NLC. The effect of plasmon resonance in an ensemble of gold nanoparticles scattered on one of the substrates of the NLC cell on the light-induced reorientation of the director was studied in [35].

In this work, the orientational instability of the director in the homeotropic cell of the NLC in an external electric field is theoretically studied. It was established that possible orientational transitions of the director from a homogeneously oriented homeotropic state to a non-homogeneous state and from a non-homogeneous to a homogeneous planar state are threshold and may be accompanied by hysteresis. The values of the threshold voltages were calculated, the existence conditions and hysteresis parameters of the specified orientational transitions of the system were determined, and their dependence on the values of the NLC cell parameters was investigated. The propagation of SPP in a three-layer Au–polymer film–NLC system is considered theoretically. The value of the effective refractive index of the SPP was calculated depending on the applied voltage, the thickness of the polymer film and the parameters of the NLC layer.

2. Director field in the NLC cell

We consider a plane cell of a nematic liquid crystal, bounded by the planes $z = 0$ and $z = L$, with the initial uniform homeotropic orientation of the director along the Oz axis (Fig. 1). The cell is in a constant uniform electric field $\mathbf{E}_0$ oriented along the Ox axis. The electric field is induced by a constant potential difference U across
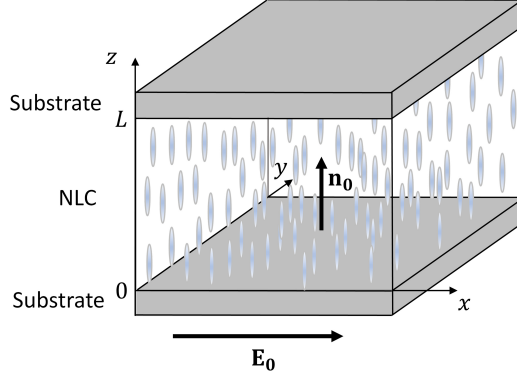
Figure 1. Initial geometry of the NLC cell. The director is initially oriented along the Oz axis, and the electric field is applied in the Ox direction.

the cell width d.

The free energy of the NLC cell can be written as:

$$F = F_{el} + F_E + F_S,$$

$$F_{el} = \frac{1}{2} \int_V \left\{ K_1 (\mathrm{div}\, \mathbf{n})^2 + K_2 (\mathbf{n} \cdot \mathrm{rot}\, \mathbf{n})^2 + K_3 [\mathbf{n} \times \mathrm{rot}\, \mathbf{n}]^2 \right\} dV,$$

$$F_E = -\frac{1}{8\pi} \int_V \mathbf{E}\hat{\epsilon}\mathbf{E}\, dV, \qquad F_S = -\frac{W}{2} \int_{S_{1,2}} (\mathbf{en})^2 \, dS. \tag{1}$$

Here F_{el} is the elastic energy of the NLC, F_E is the anisotropic contribution to the free energy of the interaction of the NLC with the electric field, F_S is the surface free energy in the form of the Rapini potential [36], K_1, K_2, K_3 are elastic constants, $\mathbf{n}$ is the director, $\mathbf{E}$ is the electric field in the NLC bulk, $\hat{\epsilon} = \epsilon_\perp \hat{\mathbf{1}} + \epsilon_a \mathbf{n} \otimes \mathbf{n}$, $\epsilon_a = \epsilon_\parallel - \epsilon_\perp > 0$ are the tensor and anisotropy of the static dielectric permittivity of the NLC, respectively, W is the energy of the NLC anchoring with the surfaces $z = 0, L$ of the bounding substrates of the cell, $\mathbf{e}$ is a unit vector directed along the Oz axis which defines the axis of easy orientation of the director on the substrates surface.

We consider plane deformations of the field of the NLC director, namely, those lying in the plane xOz. Due to the homogeneity of the system in the Oy direction, we write the director in the volume of the NLC as follows

$$\mathbf{n} = \mathbf{i} \cdot \sin\theta(z) + \mathbf{k} \cdot \cos\theta(z), \tag{2}$$

where $\mathbf{i}, \mathbf{k}$ are the unit vectors of the Cartesian coordinate system.

The variational equations for the director must be solved in conjunction with the equation for the electric field in the NLC bulk. Considering the system to be homogeneous in the Ox direction, the electric field vector in the NLC is written in the form $\mathbf{E} = (E_x(z), 0, E_z(z))$. According to the equation $\mathrm{rot}\, \mathbf{E} = 0$, the component E_x is constant and due to the electrostatic boundary conditions is equal to $E_x = U/d$. From the equation $\mathrm{div}\, \mathbf{D} = 0$ follows that the component D_z of the electric induction vector is constant and equal to 0 according to the electrostatic boundary conditions. This allows to determine the component $E_z = -\epsilon_{xz} U/(\epsilon_{zz} d)$ of the vector $\mathbf{E}$. Accordingly,

3

the free energy functional F (1) takes the form:

$$F = \frac{1}{2} \int\limits_0^L \left((K_1 \sin^2 \theta + K_3 \cos^2 \theta) \theta'^2_z - \frac{\epsilon_\| \epsilon_\perp U^2}{4\pi d^2 \epsilon_{zz}} \right) dz - \frac{W}{2} \left(\cos^2 \theta_0 + \cos^2 \theta_L \right), \quad (3)$$

where $\theta_0 = \theta(z = 0)$, $\theta_L = \theta(z = L)$ are the deviation angles of the director on the lower and upper surfaces of the cell, respectively, ϵ_{zz} is the component of the static permittivity tensor $\hat{\epsilon}$ of the NLC.

Minimization of the functional (3) by angle θ leads to the equation

$$\frac{1}{2} (K_1 - K_3) \sin 2\theta \cdot \theta'^2_z + (K_1 \sin^2 \theta + K_3 \cos^2 \theta) \theta''_{zz} + \frac{\epsilon_\| \epsilon_\perp U^2 \epsilon_{xz}}{4\pi d^2 \epsilon_{zz}^2} = 0, \quad (4)$$

and boundary conditions

$$\begin{aligned}
\left[-2(K_1 \sin^2 \theta + K_3 \cos^2 \theta) \, \theta'_z + W \sin 2\theta \right]_{z=0} &= 0, \\
\left[2(K_1 \sin^2 \theta + K_3 \cos^2 \theta) \, \theta'_z + W \sin 2\theta \right]_{z=L} &= 0,
\end{aligned} \quad (5)$$

where primes in the function θ denote the derivative with respect to the argument z.

Due to the symmetry along the z coordinate, the angle of the director must satisfy the condition $\theta(z) = \theta(L-z)$. Then, one of the boundary conditions (5) can be replaced by $\theta'(z = L/2) = 0$ or an equivalent condition $\theta(z = L/2) = \theta_m$ – the maximum angle of deviation of the director, which is reached in the middle of the cell. After integrating the equation (4) twice over z and taking into account the boundary conditions (5), we obtain the equation for the $\theta(z)$ dependence:

$$z = \frac{d}{U} \sqrt{\frac{4\pi \left(\epsilon_\perp + \epsilon_a \cos^2 \theta_m \right)}{\epsilon_\| \epsilon_\perp \epsilon_a}} \int\limits_{\theta_0}^{\theta} \sqrt{\frac{(K_1 \sin^2 \theta + K_3 \cos^2 \theta)(\epsilon_\perp + \epsilon_a \cos^2 \theta)}{\cos^2 \theta - \cos^2 \theta_m}} \, d\theta, \quad (6)$$

where the maximum angle θ_m the director and the angle θ_0 of the director on the surface are determined from the system of equations:

$$\frac{L}{2} = \frac{d}{U} \sqrt{\frac{4\pi \left(\epsilon_\perp + \epsilon_a \cos^2 \theta_m \right)}{\epsilon_\| \epsilon_\perp \epsilon_a}} \int\limits_{\theta_0}^{\theta_m} \sqrt{\frac{(K_1 \sin^2 \theta + K_3 \cos^2 \theta)(\epsilon_\perp + \epsilon_a \cos^2 \theta)}{\cos^2 \theta - \cos^2 \theta_m}} \, d\theta,$$

$$\frac{\epsilon_\| \epsilon_\perp \epsilon_a U^2}{\pi d^2} \frac{(K_1 \sin^2 \theta_0 + K_3 \cos^2 \theta_0)(\cos^2 \theta_0 - \cos^2 \theta_m)}{(\epsilon_\perp + \epsilon_a \cos^2 \theta_m)(\epsilon_\perp + \epsilon_a \cos^2 \theta_0)} = W^2 \sin^2 2\theta_0, \quad (7)$$

which can be solved only numerically.

Fig. 2 shows the calculated dependencies of the maximum angle θ_m of the director deviation and the angle θ_0 of the director at the surface of the cell on the applied voltage U for the dimensionless anchoring energy $w = WL/K_3 = 10$. The calculations were performed for the values of the NLC cell parameters $\epsilon_\| = 19$, $\epsilon_\perp = 5$, $K_1 = 11$ pN, $K_3 = 15$ pN, $L = 10$ μm, $d = 1$ mm, which are close to the typical ones [37]. As can be seen, when the voltage U in the system increases from zero, orientational transitions occur first from a uniformly oriented homeotropic state to a non-homogeneous one,
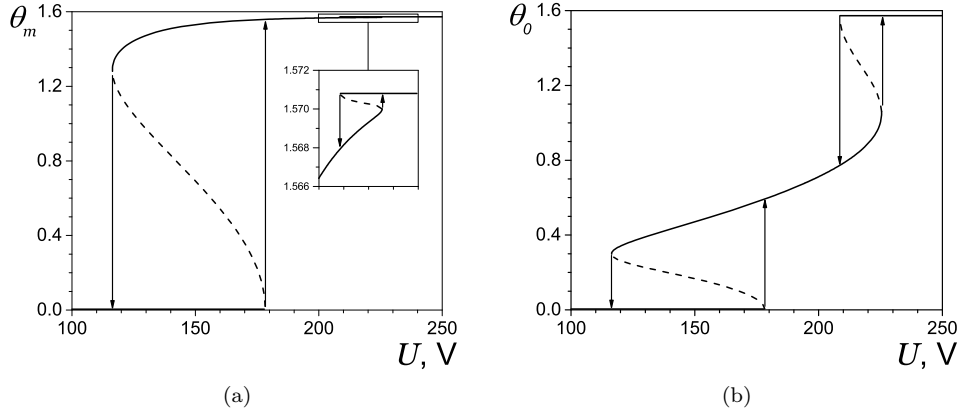
Figure 2. Dependencies of the maximum deviation angle θ_m (a) and angle θ_0 (b) of the director at the surface on the applied voltage U. Solid lines correspond to stable solutions, and dotted lines to unstable ones.

and then from a non-homogeneous to a homogeneous planar one. These transitions are of a threshold nature and may be accompanied by hysteresis (see Fig. 2). In the presence of the latter, when the voltage U reaches threshold values U_{th}, the system undergoes a sudden transition from a homogeneous state to a non-homogeneous state and vice versa. Note that when the voltage decreases, the inverse transitions also have a threshold and occur at lower voltages: $U'_{th} < U_{th}$. In general, with a change in the value of the voltage in the system, two hysteresis of orientational transitions from uniformly oriented homeotropic and planar states to non-homogeneous states can be observed.

The specified orientational transitions significantly depend not only on the voltage U, but also on the values of the anchoring energy w of the NLC with the substrate. Figure 3a shows the calculated dependence of the minimum θ_0 and maximum θ_m director angles on the anchoring energy w. With a relatively weak anchoring $w \lesssim 1$, the distribution of the director in the bulk is planar and completely determined by the electric field. When the value w increases from zero and reaches a threshold value $w_{th1} \approx 4.8$, the system switches from a uniformly oriented planar state to a non-homogeneous one. At such values of w, the influence of the surface on the orientational ordering of the NLC bulk can compete with the influence of the electric field. A further increase of w leads to a decrease in the deformations of the director's field, and when the value $w_{th2} \approx 5.4$ is reached, the system undergoes a sudden transition to the initial homeotropic state. When decreasing the values w from the region of strong anchoring $w \gtrsim 10$, the system from the homogeneous homeotropic state returns to the planarly oriented state upon reaching $w'_{th2} \approx 1.3$, thereby bypassing the non-homogeneous state. Note that the non-homogeneous state can be realized only by increasing the value w from the region of weak anchoring $w \lesssim 1$. The inverse transition from a non-homogeneous oriented state to a planar one occurs at values of the anchoring energy $w'_{th1} \approx 4.4 < w_{th1}$.

3. Orientational transitions and hysteresis

The existence conditions and hysteresis parameters (threshold values and loop width) of the transition of the system from the initial homeotropically oriented state to a non-homogeneous one and vice versa when the voltage value changes are determined

5
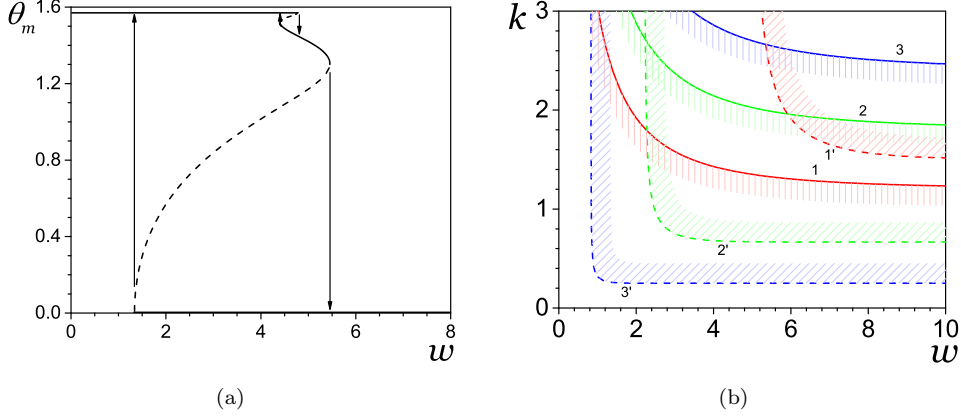
Figure 3. Dependencies of the maximum angle θ_m (a) of the director and critical values k_{th} (b) on the magnitude of the anchoring energy w. (a) $U = 100$ V. (b) k_{th1} – solid lines, k_{th2} – dashed lines. The hatching corresponds to the presence of hysteresis. $\epsilon_a/\epsilon_\parallel = 0.4\,(1, 1'), 0.6\,(2, 2'), 0.8\,(3, 3')$.

by the behavior of the system at its small deviations from the steady state $\theta = 0$. Let's consider the approximation of small angles θ. From the linearized with respect to θ equation (4) and from the boundary conditions (5), we obtain the strongest harmonic, which is the first to become unstable, in the form of $\theta(z) = \theta_m \cos\left[\varkappa_1(z/L - 1/2)\right]$. Here $\varkappa_1$ denotes the smallest positive root of the equation

$$\tan(\varkappa/2) = w/\varkappa, \qquad \text{where} \qquad \varkappa^2 = \epsilon_a \epsilon_\perp L^2 U^2/(4\pi\epsilon_\parallel K_3 d^2) \qquad (8)$$

and determines the threshold voltage U_{th1} for the transition of the system from a homeotropically oriented state to a non-homogeneous one.

Next, we substitute the mentioned solution $\theta(z)$ of the linearized problem into the free energy F (3) of the system and obtain an expansion of F in the power series by the maximum angle θ_m of director deviation: $F = \alpha\theta_m^2 + \beta\theta_m^4/2 + \gamma\theta_m^6/3 + o(\theta_m^8)$. The coefficients α, β, γ of the expansion is not presented here due to complexity of the expressions. The condition of the existence of hysteresis, as in [10], is given by the inequality $\beta|_{U=U_{th1}} < 0$, which takes the form:

$$2\left(3\epsilon_a/\epsilon_\parallel - K_1/K_3\right)\varkappa_1 + 8(\epsilon_a/\epsilon_\parallel)\sin\varkappa_1 + \left(K_1/K_3 + \epsilon_a/\epsilon_\parallel\right)\sin 2\varkappa_1 > 0. \qquad (9)$$

Note that in the case of absolutely strong anchoring ($w \to \infty$), criterion (9) is in agreement with the results in [6].

As can be seen from condition (9), the area of existence of hysteresis is determined not only by the values of voltage U and anchoring energy w, but also by the values of the parameter $k = K_1/K_3$. Fig. 3b shows numerically obtained dependences of the critical value of the parameter k_{th1} (values of k that correspond to $\beta|_{U=U_{th1}} = 0$) on the anchoring energy w for several values of the ratio $\epsilon_a/\epsilon_\parallel$. Here, when $k < k_{th1}$ the transition between the homogeneous homeotropic and non-homogeneous states is accompanied by hysteresis, and when $k > k_{th1}-$ the hysteresis is absent. An increase of the ratio $\epsilon_a/\epsilon_\parallel$ and a decrease of w leads to an expansion of range of the parameter k for which the hysteresis occurs.

Similarly, considering small deviations of the system near the steady state with $\theta = \pi/2$ we obtain the condition for the existence of hysteresis of the system transition
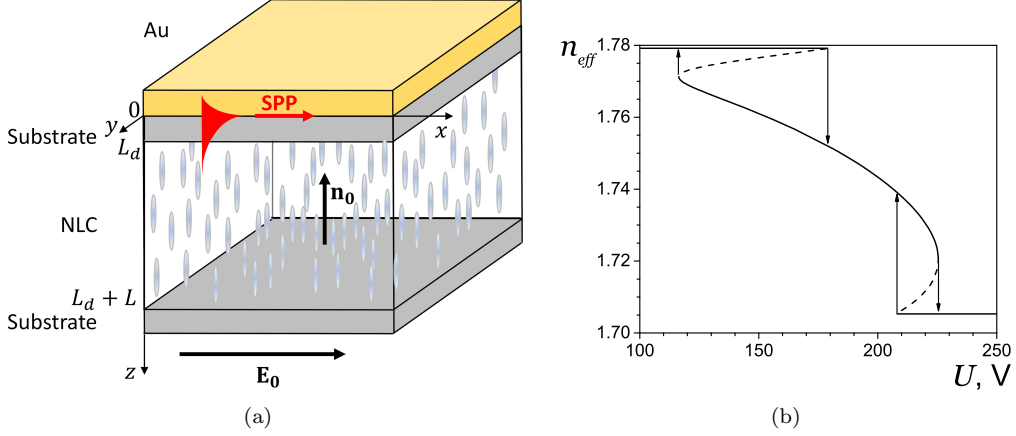
Figure 4. (a) Propagation of SPP in the Au–PF–NLC system. (b) Voltage dependence of the effective refractive index of the SPP. $L_d = 100$ nm, $w = 10$.

between the homogeneous planar and non-homogeneous states

$$-2\big(K_3/K_1 + 3\epsilon_a/\epsilon_\perp\big)\tilde{\varkappa}_1 + 8(\epsilon_a/\epsilon_\perp)\sinh\tilde{\varkappa}_1 + \big(K_3/K_1 - \epsilon_a/\epsilon_\perp\big)\sinh 2\tilde{\varkappa}_1 < 0. \quad (10)$$

Here $\tilde{\varkappa}_1$ denotes the smallest positive root of the equation

$$\tan(\tilde{\varkappa}/2) = w/(k\tilde{\varkappa}), \quad \text{where} \quad \tilde{\varkappa}^2 = \epsilon_a\epsilon_\perp\epsilon_\parallel L^2 U^2/(4\pi\epsilon_\perp^2 K_1 d^2) \quad (11)$$

and determines the value of the threshold U_{th2} for the transition of the system from a homogeneous planar state to a non-homogeneous one. Note that as the values w increase, the threshold U_{th2} increases and becomes infinitely large in the limit of absolutely strong anchoring. Therefore, in this case, the system cannot transition to a planar oriented state no matter what voltage is applied.

Dependencies of the critical value of the parameter k_{th2} on the value w are shown in Fig. 3b. Here for $k > k_{th2}$, the orientational transition between the homogeneous planar and non-homogeneous states of the system is accompanied by hysteresis, while at $k < k_{th2}$ the hysteresis is absent. As the ratio $\epsilon_a/\epsilon_\parallel$ and the parameter w increase, the range of parameter k for which the hysteresis is present expands.

Note that in the range $k_{th2} < k < k_{th1}$ (under the condition $k_{th2} < k_{th1}$) hysteresis is present for orientational transitions of the system both from a homogeneous homeotropic state to a non-homogeneous state and from a non-homogeneous to a homogeneous planar state and vice versa (see Fig. 3b). This regime in which both hysteresis loops are observed is achieved when $\epsilon_a/\epsilon_\parallel \gtrsim 0.5$. In the cases of $k < k_{th2}$ and $k > k_{th1}$ only one hysteresis is present: for the orientational transition from a homogeneous homeotropic state to a non-homogeneous state and from a homogeneous planar to a non-homogeneous state, respectively. If $\epsilon_a/\epsilon_\parallel \lesssim 0.5$ then $k_{th1} < k_{th2}$ and only one of the hysteresis of the orientational transition of the system is present for $k < k_{th1}$ and $k > k_{th2}$, with no hysteresis loops for $k_{th1} < k < k_{th2}$.

4. Surface plasmon oscillations at the NLC cell boundary

Let one of the substrates of the cell, which is a thin polymer film (PF) of thickness L_d, contact a layer of metal, for example, gold. In such Au–PF–NLC system, a surface

plasmon polariton can be excited at the Au–PF interface under appropriate conditions (see Fig. 4a). Let's write the SPP electromagnetic field in the form of a monochromatic wave of frequency ω, $\mathbf{E}(\mathbf{r}, t) = \mathbf{E}(\mathbf{r})e^{-i\omega t}$, $\mathbf{H}(\mathbf{r}, t) = \mathbf{H}(\mathbf{r})e^{-i\omega t}$. The amplitude of the oscillations of the electric and magnetic fields of the SPP decays exponentially with a distance from the interface of SPP propagation. The medium in which SPP propagates will be modeled as a three-layer optical system consisting of an isotropic homogeneous dielectric – PF, in contact with semi-infinite layers of gold on one side and NLC on the other. In order to take into account the effect of anisotropy and heterogeneity of the NLC media on the propagation of SPP, we will use the perturbation theory [31]. In the zeroth approximation of this theory, we find the form of the electric $\mathbf{E}(\mathbf{r})$ and magnetic $\mathbf{H}(\mathbf{r})$ fields of the SPP as solutions of the system of Maxwell's equations in a homogeneous isotropic media with dielectric permittivity

$$\varepsilon_0(z) = \varepsilon_m \chi(-z) + \varepsilon_d \chi(z), \tag{12}$$

where ε_m, ε_d are the dielectric constants of the metal and polymer at the SPP propagation frequency, respectively, $\chi(t) = 0$ if $t <= 0$ and $\chi(t) = 1$ if $t > 0$. Here, the axis of the Cartesian coordinate system is directed toward the NLC, and the axis Ox is oriented in the direction of SPP propagation along the Au–PF contact boundary. The zeroth approximation for the SPP electric and magnetic field vectors takes the form

$$\mathbf{E}_0(\mathbf{r}) = \frac{cA_0}{\omega\varepsilon_{m,d}}\left(\pm i\beta_{m,d}, 0, -k_{0x}\right)e^{i\mathbf{k}_0\mathbf{r}}, \qquad \mathbf{H}_0(\mathbf{r}) = \left(0, A_0, 0\right)e^{i\mathbf{k}_0\mathbf{r}}, \tag{13}$$

where A_0 is the amplitude factor, indices m, d denote metal ($z < 0$) and polymer ($z > 0$), respectively. The components of the wave vector $\mathbf{k}_0 = (k_{0x}, 0, \pm i\beta_{m,d})$ are expressed in terms of dielectric permittivities $\varepsilon_{m,d}$:

$$k_{0x} = \frac{\omega}{c}\sqrt{\frac{\varepsilon_d\varepsilon_m}{\varepsilon_d + \varepsilon_m}}, \qquad \beta_m = \frac{\omega}{c}\sqrt{-\frac{\varepsilon_m^2}{\varepsilon_d + \varepsilon_m}}, \qquad \beta_d = \frac{\omega}{c}\sqrt{-\frac{\varepsilon_d^2}{\varepsilon_d + \varepsilon_m}}. \tag{14}$$

Anisotropy and inhomogeneity of the NLC layer are taken into account as a perturbation, so that the dielectric constant of the considered three-layer system model becomes

$$\hat{\varepsilon}(z) = \varepsilon_0(z)\hat{\mathbf{1}} + \eta\Delta\hat{\varepsilon}(z), \quad \text{where} \quad \Delta\hat{\varepsilon}(z) = \left[\varepsilon_a\left(\mathbf{n}\otimes\mathbf{n} - \hat{\mathbf{1}}/3\right) + \varepsilon_c\hat{\mathbf{1}}\right]\chi(z - L_d). \tag{15}$$

Here $\varepsilon_a = \varepsilon_\parallel - \varepsilon_\perp$, $\varepsilon_c = (\varepsilon_\perp + 2\varepsilon_\parallel)/3 - \varepsilon_d$, $\varepsilon_\parallel$ and $\varepsilon_\perp$ are parallel and perpendicular component of the dielectric permittivity tensor, respectively, of a homogeneous NLC at the frequency ω, $\eta \ll 1$.

Next, we find the solution of the system of Maxwell's equations in the media with the dielectric constant tensor $\hat{\varepsilon}(z)$ (15). The SPP electric and magnetic field vectors can be found as an expansion with respect to the small parameter η:

$$\mathbf{E} = \mathbf{E}_0 + \eta\mathbf{E}_1 + o(\eta^2), \qquad \mathbf{H} = \mathbf{H}_0 + \eta\mathbf{H}_1 + o(\eta^2), \tag{16}$$

where the vectors $\mathbf{E}_0$ and $\mathbf{H}_0$ were found earlier (13) within the isotropic approximation, and the corrections $\mathbf{E}_1$ and $\mathbf{H}_1$ take into account the presence of the NLC layer. Solving the equations for $\mathbf{E}_1$ and $\mathbf{H}_1$ in the linear by η approximation we find the

correction to the zeroth approximation $n_{eff}^0 = ck_{0x}/\omega$ of the effective refractive index of SPP:

$$n_{eff} = \frac{c}{\omega} k_{0x} \big(1 + Ke^{-2\beta_d L_d}\big), \tag{17}$$

where

$$K = \frac{\varepsilon_m \varepsilon_c}{2\left(\varepsilon_d + \varepsilon_m\right)\varepsilon_d} - \frac{\left(\varepsilon_d + 2\varepsilon_m\right)\varepsilon_m \varepsilon_a}{6\varepsilon_d \left(\varepsilon_d^2 - \varepsilon_m^2\right)} + \frac{\varepsilon_m \varepsilon_a}{2\varepsilon_d \left(\varepsilon_d - \varepsilon_m\right)} - \frac{\varepsilon_m \varepsilon_a e^{2\beta_d L_d}}{\varepsilon_d \left(\varepsilon_d - \varepsilon_m\right)} \int\limits_{L_d}^{\infty} \sin^2\big[\theta(z - L_d)\big] e^{-2\beta_d z}\, dz$$

and can be calculated for an arbitrary director profile in the NLC layer. Fig. 4b shows the calculated dependence of the effective refractive index of SPP on the applied voltage U. Calculations were made for the following values of the dielectric permittivities of gold $\varepsilon_m = -26.43$, PF $\varepsilon_d = 2.81$ and NLC E7 $\varepsilon_\parallel = n_e^2$, $\varepsilon_\perp = n_o^2$ (here $n_e = 1.71$, $n_o = 1.51$), which correspond to the wavelength of $\lambda = 800$ nm [33,38].We note that although in the presented theoretical study the layer of gold was considered semi-infinite, the value of the dielectric constant of gold, taken for calculation, corresponds to the experimentally measured in [33] for a gold film with a thickness of 40 nm.

When the applied voltage increases from 0 to U_{th1}, the effective refractive index of the SPP is constant $n_{eff} \approx 1.78$, since the NLC is oriented homeotropically across the whole volume (see Fig. 5a). When the voltage U reaches the threshold value U_{th1}, the value n_{eff} undergoes a sudden decrease, which is a consequence of the orientational transition of the NLC director field from the homeotropically oriented state to the non-homogeneous one. A further increase of U leads to a gradual decrease of n_{eff}, and when the voltage reaches the threshold value U_{th2}, the value n_{eff} abruptly drops to $n_{eff} \approx 1.71$. Such a drop is caused by the orientational transition of the NLC director from a non-homogeneous state to a uniform planar one. A further increase in voltage does not change the values of n_{eff}, since the uniform orientation of the director in the NLC layer is preserved. In general, an increase of the voltage U leads to a decrease of n_{eff}. This is explained by the fact that the director in the NLC layer generally reorients from the homeotropic state to the planar state. At the same time, the oscillations of the SPP electric field vector $\mathbf{E}$, in particular in the direction of Oz, feel a decrease of the refractive index of the NLC from n_e to n_o. When the voltage is reduced, abrupt changes of n_{eff} of SPP occur at lower voltages U showing therefore hysteresis-like behavior. Apparently, the two hysteresis of the dependence $n_{eff}(U)$ are a consequence of the presence of hysteresis of dependence $\theta_0(U)$ (Fig. 2b), since the value n_{eff} of SPP is determined primarily by the value of the angle of the NLC director near the surface where the SPP is excited. An increase of the anchoring energy w leads to a shift of both hysteresis in the direction of higher voltage U. At the same time, the amplitude of the hysteresis between homeotropic and non-homogeneous states increases and the width of the other hysteresis decreases.

Fig. 5a shows the dependence of n_{eff} of SPP on the applied voltage for different SPP wavelengths. As the wavelength increases, the range of values for n_{eff} expands and shifts towards lower values of n_{eff}.

The dependence of the n_{eff} of SPP on the applied voltage for different PF thicknesses is shown in Fig. 5b. As the PF thickness increases, the range of values of n_{eff} of SPP narrows. The point ($U \approx 117$ V, $n_{eff} \approx 1.77$) in the Fig. 5b, where the curves corresponding to different PF thicknesses intersect, can be explained as follows. If the value of the PF refractive index n_d satisfies the condition $n_o < n_d < n_e$, then there is
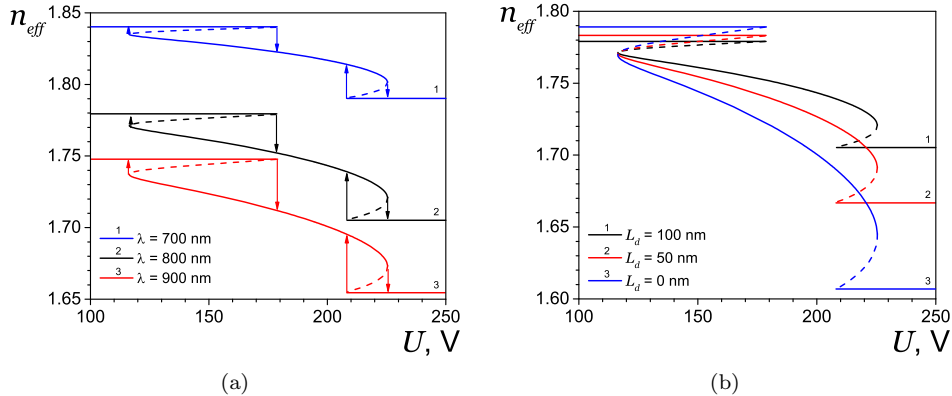
Figure 5. Dependence of the effective refractive index of SPP on the applied voltage at different wavelengths (a) and polymer film thicknesses (b).

a distribution of the director field for which refractive index of the near-surface layer of the NLC is close to n_d. Under such conditions the dependence on the PF thickness in the system disappears.

5. Summary

The electrically induced orientational instability of the director in the cell of a homeotropically oriented NLC was theoretically investigated. It has been established that when the value of the applied voltage increases from zero, orientational transitions from the uniform homeotropic state to the non-homogeneous one, and then from the non-homogeneous to the homogeneous planar state occur in the system. The influence of system parameters on these transitions, particularly the anchoring energy w of the NLC with the surface, the ratios $k = K_1/K_3$ of elastic and $\epsilon_a/\epsilon_\parallel$ dielectric constants of NLC was investigated. The mentioned orientation transitions have thresholds and may be accompanied by hysteresis. In the presence of the latter, when the voltage U reaches threshold values U_{th}, the system jumps from a homogeneous state to a non-homogeneous state and vice versa. When the applied voltage decreases, the inverse transitions occur at lower threshold voltage values: $U'_{th} < U_{th}$. It was established that the planar state is achieved only under the condition of finiteness of the anchoring energy w and is unreachable in the case of absolutely strong anchoring. When the anchoring energy w is changed at a constant voltage U, the non-homogeneous state can be realized only with an increase in the value of the anchoring energy from the region of weak anchoring $w \lesssim 1$. When the values w decrease from the region of strong anchoring $w \gtrsim 10$, the system reorients from the homogeneous homeotropic state to the planar state, bypassing the non-homogeneous state.

The existence conditions and parameters of the hysteresis of orientational transitions of the system when the value of applied voltage is varied have been established. The critical values k_{th1} and k_{th2} of a parameter k have been established such that for $k < k_{th1}$ the orientational transition between the homeotropic and non-homogeneous states is accompanied by hysteresis, and for $k > k_{th1}$ there is no hysteresis. Similarly, the hysteresis of the orientational transition of the system from the planar state to the non-homogeneous state is present for $k > k_{th2}$ and absent otherwise. As the value w of the anchoring energy increases, the range of parameter k for which the hysteresis of the

10

system transition from the homeotropic state to the non-homogeneous state is present narrows, and expands for the transition from the planar state to the non-homogeneous state. As the anchoring energy w increases, the amplitude of the hysteresis increases for the transition between the homeotropic and non-homogeneous states, and the width of the other hysteresis decreases.

For ratio $\epsilon_a/\epsilon_\parallel > 0.5$ in case of $k_{th2} < k < k_{th1}$ the transitions between all states have a hysteresis (the double-hysteresis regime can occur only if $k_{th2} < k_{th1}$). For $k < k_{th2}$ and $k > k_{th1}$ there is only one of the hysteresis of the orientational transition: from the homeotropic state to the non-homogeneous state and from the planar to the non-homogeneous state, respectively. If $\epsilon_a/\epsilon_\parallel \lesssim 0.5$, then the condition $k_{th1} < k_{th2}$ is fulfilled and only one of the hysteresis of the orientational transition of the system is present in the regions $k < k_{th1}$ and $k > k_{th2}$. Finally, for $k_{th1} < k < k_{th2}$ there are no hysteresis loops at all.

The influence of the external electric field changes on the parameters and conditions of SPP propagation in the Au–polymer film–NLC system was considered. The value of the effective refractive index n_{eff} of the SPP was calculated and its dependence on the values of the applied voltage U, the thickness L_d of the polymer film and the parameters of the NLC layer was investigated. It was established that the value of the effective refractive index n_{eff} of SPP increases with an increase of the anchoring energy w and with a decrease in the voltage U and wavelength λ of the SPP. The range of possible values of n_{eff} of SPP expands as the thickness L_d of the polymer film decreases and the wavelength λ increases.

References

[1] De Gennes PG, Prost J. The Physics of Liquid Crystals. Oxford: Oxford University Press. 1993:83.

[2] Zel'dovich BY, Tabiryan N, Chilingaryan YS. Freedericksz transitions induced by light fields. JETP. 1981;54;32-41.

[3] Durbin SD, Arakelian SM, Shen YR. Optical-Field-Induced Birefringence and Freedericksz Transition in a Nematic Liquid Crystal. Phys Rev Lett. 1981;47(19);1411-1419.

[4] Zolotko AS, Kitaeva VF, Kroo N et al. The effect of an optical field on the nematic phase of the liquid crystal OCBP. JETP Lett. 1980;32(2);158-162.

[5] Brasselet E, Lherbier A, Dubé LJ. Transverse nonlocal effects in optical reorientation of Nematic Liquid Crystals. J Opt Soc Am B. 2006;23:36.

[6] Frisken BJ, Palffy-Muhoray P. Electric-field-induced twist and bend Freedericksz transitions in nematic liquid crystals. Phys Rev A. 1989;39(3);1513-1518.

[7] E. Brasselet, B. Piccirillo, E. Santamato, Three-dimensional model for light-induced chaotic rotations in liquid crystals under spin and orbital angular momentum transfer processes. Phys. Rev. E. 2008;78;031703.

[8] Budagovsky I, Pavlov D, Shvetsov S et al. First-order light-induced orientation transition in nematic liquid crystal in the presence of low-frequency electric field. Appl Phys Lett. 2012;101;021112,1-3.

[9] Vella A, Piccirillo B, Santamato E. Coupled-mode approach to the nonlinear dynamics induced by an elliptically polarized laser field in liquid crystals at normal incidence. Phys Rev E. 2002;65:031706.

[10] Ong HL. Optically induced Freedericksz transition and bistability in a nematic liquid crystal. Phys Rev A. 1983;28(4);2393-2407.

[11] D'Alessandro G, Wheeler AA. Bistability of liquid crystal microcavities. Phys Rev A. 2003;67:023816.

[12] Ilyina V, Cox SJ, Sluckin TJ. A computational approach to the optical Fréedericksz

transition. Opt Comm. 2006;260:474–480.

[13] U.A. Laudyn, A.E. Miroshnichenko, W. Krolikowski et al. Observation of light-induced reorientational effects in periodic structures with planar nematic-liquid-crystal defects. Appl. Phys. Lett., 2008:92:203304.

[14] Miroshnichenko AE, Brasselet E, Kivshar YS. Light-induced orientational effects in periodic photonic structures with pure and dye-doped nematic liquid crystal defects. Phys Rev A. 2008;78:053823.

[15] Ledney MF, Tarnavskyy OS, Lesiuk AI, Reshetnyak VY. Interaction of electromagnetic waves in nematic waveguide. Mol Cryst Liq Cryst. 2016:638(1):1-16.

[16] Sutormin VS, Krakhalev MN, Prishchepa OO et al. Electro-optical response of an ionic-surfactant-doped nematic cell with homeoplanar–twisted configuration transition. Optic. Mater. Expr. 2014:4(4):810-815.

[17] Lesiuk AI, Ledney MF, Tarnavskyy OS. Orientational instability of nematic liquid crystal in a homeotropic cell with boundary conditions controlled by an electric field. Liq Cryst. 2019:46(3):469-483.

[18] Tarnavskyy OS, Ledney MF. Orientational instability of the director in a nematic cell caused by electro-induced anchoring modification. Cond Matt Phys. 2021:24(1):13601,1–14.

[19] Sprokel GJ, Santo R, Swalen JD. Determination of the surface tilt angle by attenuated total reflection. Mol Cryst Liq Cryst. 1981;68(1-4);977-986.

[20] Welford KR, Sambles JR, Clark MG. Guided modes and surface plasmon-polaritons observed with a nematic liquid-crystal using attenuated total reflection. Liq Cryst. 1987;2(1);91-105.

[21] Sprokel GJ. The rflectivity of a liquid-crystal cell in a surface-plasmon experiment. Mol Cryst Liq Cryst. 1981;68(1-4);987-993.

[22] Welford KR, Sambles JR. Detection of surface director reorientation in a nematic liquid-crystal. Appl Phys Lett. 1987;50(14);871-873.

[23] Caldwell ME, Yeatman EM. Surface-plasmon spatial light modulators based on liquid-crystal. Appl Opt. 1992;31(20);3880-3891.

[24] Wang Y. Voltage-induced color-selective absorption with surface-plasmons. Appl Phys Lett. 1995;67(19);2759-2761.

[25] Yang FZ, Sambles JR. Microwave liquid crystal wavelength selector. Appl Phys Lett. 2001;79(22);3717-3719.

[26] Wang Y, Russell SD, Shimabukuro RL. Voltage-induced broad-spectrum reflectivity change with surface-plasmon waves. J Appl Phys. 2005;97(2).

[27] Dickson W, Wurtz GA, Evans PR, et al. Electronically controlled surface plasmon dispersion and optical transmission through metallic hole arrays using liquid crystal. Nano Lett. 2008;8:281–286.

[28] Bortolozzo U, Residori S, Huignard JP. Beam coupling in photorefractive liquid crystal light valves. J Phys D. 2008;41;224007.

[29] Buchnev O, Dyadyusha A, Kaczmarek M, et al. Enhanced two-beam coupling in colloids of ferro- electric nanoparticles in liquid crystals. J Opt Soc Am B. 2007;24;1512–1516.

[30] Cook G, Glushchenko AV, Reshetnyak V, et al. Nanoparticle doped organic- inorganic hybrid photorefractives. Opt Express. 2008;16;4015–4022.

[31] Daly K, Abbott S, D'Alessandro G, et al. Theory of hybrid photorefractive plasmonic liquid crystal cells. J Opt Soc Am B. 2011;28;1874-1881.

[32] Abbott SB, Daly KR, D'Alessandro G, et al. Photorefractive control of surface plasmon polaritons in a hybrid liquid crystal cell. Opt Lett. 2012;37;2436-2438.

[33] Abbott SB. Energy transfer between surface plasmon polariton modes with hybrid photorefractive liquid crystal cells [dissertation]. School of Physics and Astronomy: University of Southampton; 2012.

[34] Daly KR, Light-matter interaction in liquid crystal cells [dissertation]. School of Mathematics: University of Southampton; 2011.

[35] Lesiuk AI, Ledney MF, Reshetnyak VYu. Light-induced Fredericks transition in the ne-

matic liquid crystal cell with plasmonic nanoparticles at a cell bounding substrate. Phys Rev E. 2022:106(2):024706,1-6.

[36] Rapini A, Papoular M. Distorsion d'une lamelle nematique sous champ magnetique conditions d'ancrage aux parois. Le Journal de Physique Colloques. 1969;30(C4);54-67.

[37] Blinov LM, Chigrinov VG. Electrooptic effects in liquid crystal materials. New York (NY): Springer Verlag; 1994:361.

[38] Tkachenko V, Abbate G, Marino A, et al. Nematic liquid crystal optical dispersion in the visible-near Infrared Range. Mol Cryst Liq Cryst. 2006;454;263-271.